Perfectly Matched Layer with Mixed Spectral Elements for the Propagation of Linearized Water Waves

Gary Cohen, Sébastien Imperiale

Perfectly Matched Layer with Mixed Spectral Elements for the Propagation of Linearized Water Waves

Gary Cohen, Sébastien Imperiale *

INRIA, Domaine de Voluceau, Rocquencourt - BP 105, 78153 Le Chesnay Cedex, France

Abstract. After setting a mixed formulation for the propagation of linearized water waves problem, we define its spectral element approximation. Then, in order to take into account unbounded domains, we construct absorbing perfectly matched layer for the problem. We approximate these perfectly matched layer by mixed spectral elements and show their stability using the 'frozen coefficient' technique. Finally, numerical results will prove the efficiency of the perfectly matched layer compared to classical absorbing boundary conditions.

AMS subject classifications: 35J05

PACS (2006): 41.20.cv 43.20.Hq
Key words: Linearized water waves, Perfectly matched layer, Mixed finite elements.

1 Introduction

We start with the equations presented in [1] which model gravity wave generation and propagation in water, in its complete form, it reads as solving an homogeneous Laplacian problem in water coupled with a non linear boundary condition on the surface depending on time . A simpler model is obtained by linearizing the surface condition in order to only describe the propagation of the gravity wave, which is sufficient for waves of small amplitudes compared to the deepness of the bottom and the wavelength. The purpose of this paper is to develop original absorbing perfectly matched layers (PML) to take into account the propagation of linearized water waves (LWW) problem in unbounded domains and to present their finite element discretization. PML was introduced by Bérenger [2] for hyperbolic problems. In this paper we extend these ideas to a strongly elliptic problem. We will present the approximation of the PML for the LWW equations by high order mixed spectral elements with Legendre-Gauss-Lobatto points. This approach was successfully applied to the acoustics and linear elastodynamic equations [3], [4]. For classical transient equations, this approximation is fundamental since it provides mass-lumping which

*Corresponding author. *Email addresses:* sebastien.imperiale@inria.fr (S. Imperiale)

substantially reduces the cost of the method. In our case, the mixed form of the spectral element method enables a simple writing of the PML system, without adding extra variables (as in [2] and [5]), and leads to a low storage and factorization of the propagation operator (the stiffness matrix). This second property provides an efficient algorithm for wave equations in frequency domain [6] . This factorization can be even more efficient for a Laplacian problem, which justifies our approximation for the LWW problem. The stability of our PML is also studied. Whereas stability issues are often a difficult question (especially for elastodynamic waves), in this article we manage to prove the stability of the PML at a continuous level. We also present 2D numerical results that shows that previously designed high order absorbing condition (see [7]) are long time unstable, whereas the PML are long time stable at a discrete level.

Our paper is divided into four parts: In a first part, we introduce the mixed form of the problem and its variational formulation. In a second part, we construct its approximation by spectral elements whose principle is recalled. Then, we present the discrete formulation by pointing out the sparse and low storage character of the matrices involved. In a third part, after discussing the stability of the absorbing boundary conditions (ABC) of first order for taking into account unbounded domains [7], we construct perfectly matched layers using the reformulation introduced by Chew and Weedon [5]. Then, we show how to apply the mixed spectral element method to these PML. Finally we show the stability of the continuous PML by using a frozen coefficient technique as in [8]. The fourth part is devoted to numerical experiments which prove the stability and the efficiency in terms of reflections of the PML compared to the first order ABC.

2 The Continuous Problem

2.1 Classical Formulation

Let Ω be an open domain of $\mathbb{R}^d$ $(d=2,3)$ and Γ_S, Γ_B and Γ_h three subsets providing a partition of $\partial\Omega$.

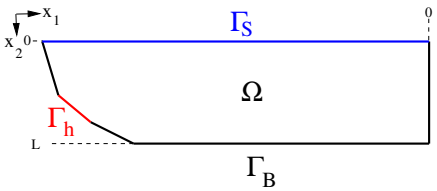

With these notations, the continuous problem reads as follows:

$$\Delta\Phi=0 \text{ in } \Omega, \quad \frac{\partial^2\Phi}{\partial t^2}+g\frac{\partial\Phi}{\partial n}=0 \text{ on } \Gamma_S, \quad \frac{\partial\Phi}{\partial n}=h \text{ on } \Gamma_h, \quad \frac{\partial\Phi}{\partial n}=0 \text{ on } \Gamma_B. \tag{2.1}$$

where h is a given function of x and t, g is the gravitation constant and Φ is the velocity potential in the fluid. On the other hand, $\partial/\partial n = \vec{n}\cdot\nabla$, $\vec{n}$ being the outward normal unit on $\partial\Omega$. In the following we consider zero initial condition. The shape of the surface ocean is given at any time by

$$\eta(x,t) = \frac{1}{g}\frac{\partial}{\partial t}\Phi(x,0,t). \tag{2.2}$$

This problem has its evolution term on its boundary, which must be coupled with the equation in Ω. We write a proper variational formulation, in which $\Phi \in H^1(\Omega)$. We multiply by $H^1(\Omega)$ test functions the first equation of (2.1), integrate by parts and replace the boundary terms. We have to find $\Phi \in H^1(\Omega)$ such that

$$\int_\Omega \nabla\Phi\cdot\nabla\varphi \mathrm{d}\vec{x} + \frac{1}{g}\frac{\mathrm{d}^2}{\mathrm{d}t^2}\int_{\Gamma_S}\Phi\varphi \mathrm{d}\sigma = \int_{\Gamma_h} h\varphi \mathrm{d}\sigma, \quad \forall\varphi \in H^1(\Omega). \tag{2.3}$$

2.2 Mixed Formulation

The first step towards the construction of our approximation is to reformulate equations (2.1) as the following system:

$$\begin{gathered} \nabla\cdot\vec{v} = 0 \text{ in } \Omega, \quad \vec{v} = \nabla\Phi \text{ in } \Omega, \\ \frac{\partial^2\Phi}{\partial t^2} + g\vec{v}\cdot\vec{n} = 0 \text{ on } \Gamma_S, \quad \vec{v}\cdot\vec{n} = h \text{ on } \Gamma_h, \quad \vec{v}\cdot\vec{n} = 0 \text{ on } \Gamma_B. \end{gathered} \tag{2.4}$$

As previously, the second step is the definition of a proper variational formulation of the mixed formulation. We seek for $\Phi \in H^1(\Omega)$ and $\vec{v} \in \left[L^2(\Omega)\right]^d$. Again, we integrate by parts the first equation and we replace the boundary terms by (2.4). We finally get

$$\begin{aligned} -\int_\Omega \vec{v}\cdot\nabla\varphi \mathrm{d}\vec{x} + \frac{1}{g}\frac{\mathrm{d}^2}{\mathrm{d}t^2}\int_{\Gamma_S}\Phi\varphi \mathrm{d}\sigma &= \int_{\Gamma_h} h\varphi \mathrm{d}\sigma \qquad \forall\varphi \in H^1(\Omega), \\ \int_\Omega \vec{v}\cdot\vec{\psi} \mathrm{d}\vec{x} &= \int_\Omega \nabla\Phi\cdot\vec{\psi} \mathrm{d}\vec{x} \qquad \forall\vec{\psi} \in \left[L^2(\Omega)\right]^d. \end{aligned} \tag{2.5}$$

3 Construction of the Discrete Formulation

3.1 Approximation Spaces

In order to define the approximate spaces, let $\widehat{K} = [0,1]^d$ be the squared or cubic reference element, $\vec{\hat{x}} \in \widehat{K}$ and $\mathcal{M}_h$ be a mesh of Ω composed of N_e quadrilaterals in 2D and of hexahedra in 3D denoted K_j. $\vec{F}_j = (F_{j,1}...F_{j,d})$ is the mapping such that $\vec{F}_j(\widehat{K}) = K_j$, we note DF_j the jacobian matrix of F_j and J_j its determinant. On this mesh, we define the following subspace of $H^1(\Omega)$:

$$U_h^r = \left\{ v_h \in H^1(\Omega) \text{ such that } v_{h|_{K_j}} \circ \vec{F}_j \in Q_r \right\}, \tag{3.1}$$

and the subspace of $\left[L^2(\Omega)\right]^d$ defined as

$$\mathbf{V}_h^r = \{\vec{v}_h \in \left[L^2(\Omega)\right]^2 \text{ such that } \forall K_j \in \mathcal{M}_h, |J_j| DF_j^{-1} \vec{v}_h|_{K_j} \circ \vec{F}_j \in [Q_r]^d\}, \tag{3.2}$$

where Q_r is the classical polynomial of total degree at most r. For elements with straight edges, the mapping $\vec{F}_j$ can be easily derived from the Q_1 basis functions on $\widehat{K}$. The use of elements derived from $\widehat{K}$ is very convenient since basis functions $\hat{\varphi}$ in 2D or 3D on $\widehat{K}$ can be written as a product of one-dimensional basis functions as follows:

$$\hat{\varphi}_{\vec{j}}(\vec{\hat{x}}) = \prod_{k=1}^{d} \hat{\varphi}_{j_k}(\hat{x}_k). \tag{3.3}$$

$\{\hat{\xi}_p\}$ being a 1D set of $r+1$ interpolation points, which are the Legendre Gauss-Lobatto (LGL) quadrature points. The functions $\hat{\varphi}_{j_k}$ satisfy the relation

$$\hat{\varphi}_{j_k}(\hat{\xi}_p) = \delta_{j_k p}, \quad \forall p = 1..r+1. \tag{3.4}$$

where $\delta_{j_k p}$ is the Kronecker symbol. In what follows the integral with the upper script LGL are computed using the LGL quadrature points. More details about the definition of the approximation spaces and the quadrature formulae can be found in [3].

3.2 The Semi-Discrete Problem in Space

With the above notations, the approximate problem reads:

Find $\Phi_h \in U_h^r$ and $\vec{v}_h \in \mathbf{V}_h^r$ such that

$$\begin{aligned} \int_\Omega^{LGL} \vec{v}_h \cdot \nabla \varphi_h \mathrm{d}\vec{x} + \frac{1}{g} \frac{\mathrm{d}^2}{\mathrm{d}t^2} \int_{\Gamma_S}^{LGL} \Phi_h \varphi_h \mathrm{d}\sigma &= \int_{\Gamma_h}^{LGL} h \varphi_h \mathrm{d}\sigma \qquad \forall \varphi_h \in U_h^r, \\ \int_\Omega^{LGL} \vec{v}_h \cdot \vec{\psi}_h \mathrm{d}\vec{x} &= \int_\Omega^{LGL} \nabla \Phi_h \cdot \vec{\psi}_h \mathrm{d}\vec{x} \qquad \forall \vec{\psi}_h \in \mathbf{V}_h^r. \end{aligned} \tag{3.5}$$

By computing all the integrals of (3.5) using a LGL quadrature rule of order r (which is exact for polynomials of order $2r-1$), we get the following semi-discrete problem in space:

Find $U = (u_i)_{i=1}^{N_u}$ and $V = (v_i)_{i=1}^{N_e(r+1)^d}$ such that

$$R_h V + \frac{1}{g} \frac{\mathrm{d}^2}{\mathrm{d}t^2} D_h^\gamma U - H = 0, \quad B_h V = R_h^* U, \tag{3.6}$$

where R_h^* is the transposed matrix of R_h and

$$R_{h,ij} = \int_\Omega^{LGL} \vec{\psi}_j . \nabla \varphi_i \mathrm{d}x, \quad B_{h,ij} = \int_\Omega^{LGL} \vec{\psi}_j \vec{\psi}_j \mathrm{d}x, \quad D_{h,ij}^\gamma = \int_{\Gamma_S}^{LGL} \varphi_j \varphi_i \mathrm{d}x. \tag{3.7}$$

We now list some important properties of the discretization:

1. U and V are the degree of freedom (D.O.F) vectors corresponding to Φ_h and $\vec{v}_h$ respectively, H is the right-hand side,
2. R_h is a stiffness matrix whose definition requires its knowledge on $\widehat{K}$ only,
3. D_h^γ is a diagonal matrix such that $d_{ij}=a_{ij}\delta_{ij}\delta_{\vec{x}_i\in\Gamma_S}$, $\delta_{\vec{x}_i\in\Gamma_S}$ being equal to one if the location $\vec{x}_i$ corresponding to the ith D.O.F is on Γ_S zero otherwise,
4. B_h is $d\times d$ block-diagonal symmetric matrix.

Property 2 comes from the following identity

$$\forall K_j\in\mathcal{M}_h,\quad \forall\varphi_h\in U_h^r,\quad \forall\vec{\psi}_h\in\vec{V}_h^r,\quad \int_{K_j}^{LGL}\nabla\varphi_h\cdot\vec{\psi}_h\,\mathrm{d}\vec{x}=\int_{\widehat{K}}^{LGL}\widehat{\nabla}\widehat{\varphi}_h\cdot\widehat{\vec{\psi}}_h\,\mathrm{d}\widehat{\vec{x}}. \tag{3.8}$$

where $\widehat{\nabla}$ is the ∇ operator in $\widehat{\vec{x}}$ coordinates, $J_j=\det DF_j$ and $\widehat{\vec{\psi}}_h=|J_j|DF_j^{-1}\vec{\psi}_h|_{K_j}\circ\vec{F}_j$. This justifies the somehow strange definition of $\vec{V}_h^r$. On the other hand, if R_h^* is computed element by element, we do not need to store it. This kind of computation become more and more efficient as the order increase. The property 3 and 4 are crucial, it corresponds to mass lumping on discrete H^1 and $[L^2]^d$ spaces and will enable an easy implementation of the perfectly matched layer.

Remark: As proven in [3], we have

$$K_h=R_hB_h^{-1}R_h^*, \tag{3.9}$$

where K_h is the stiffness matrix of the following approximate variational formulation: Find $\Phi_h\in U_h^r$ such that

$$\int_\Omega^{LGL}\nabla\Phi_h\cdot\nabla\varphi_h\,\mathrm{d}\vec{x}+\frac{1}{g}\frac{\mathrm{d}^2}{\mathrm{d}t^2}\int_{\Gamma_S}^{LGL}\Phi_h\varphi_h\,\mathrm{d}\sigma=\int_{\Gamma_h}^{LGL}h\varphi_h\,\mathrm{d}\sigma,\quad\forall\varphi_h\in U_h^r. \tag{3.10}$$

This shows that (3.6) is a reformulation of the spectral element approximation of (2.1).

3.3 The Fully Discrete Problem

The discretization in time is made by a centered θ-scheme as follows

$$R_h(\theta V^{n+1}+(1-2\theta)V^n+\theta V^{n-1})+\frac{1}{g}D_h^\gamma\frac{U^{n+1}-2U^n+U^{n-1}}{\Delta t^2}-H^n=0, \tag{3.11}$$

$$B_hV^n=R_h^*U^n. \tag{3.12}$$

where Δt is the time-step and $\theta\geq 1/4$. For the sake of simplicity we choose to take $\theta=1/2$ (as it kills the centered term) but every choice of $\theta\geq 1/4$ will provide an unconditionally

stable scheme The choice $\theta<1/4$ gives either an ill-posed problem ($\theta=0$) or an unstable scheme. With $\theta=1/2$, taking into account (3.9), the solution of (3.11)-(3.12) reads

$$U^{n+1}=g\Delta t^2(D_h^\gamma-\frac{g\Delta t^2}{2}K_h)^{-1}\big(\frac{1}{2}K_hU^{n-1}+\frac{1}{g\Delta t^2}D_h^\gamma(2U^n-U^{n-1})+H^n\big). \tag{3.13}$$

3.4 Algorithmic issues

Computing the solution of (3.13) requires an inversion of a discrete Laplace operator at each time-step. When a factorization cannot be achieved, the resolution is classically made by a conjugate gradient method which is based on a recurrent product of matrix $D_h^\gamma+\frac{g\Delta t^2}{2}K_h$ by a vector p_k. By using (3.9), this product π_k can be decomposed as follows

$$q_k=B_h^{-1}R_h^*p_k \quad \text{then} \quad \pi_k=-\frac{g\Delta t^2}{2}R_hq_k+D_h^\gamma p_k. \tag{3.14}$$

As shown in [3] such a decomposition leads to a low-storage and fast matrix-vector product for high-order approximation. For preconditioning, a multigrid algorithm can be used i.e, the inverse of the matrix is approximate by the inverse of a matrix coming from the a lower order approximation. It has been shown in [6] to be an efficient technique on helmoltz problem (especially in 3D) and it can naturally be extended to a laplace problem.

4 Unbounded Domains

4.1 Absorbing Boundary Conditions

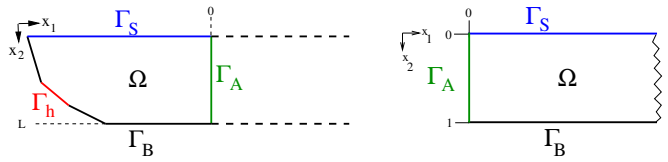

Figure 1: We look for a DtN on Γ_A. The solution on a semi-infinite rectangle is computed analytically.

The key idea to write an ABC is to look for a Dirichlet to Neumann operator. The domain after Γ_A is a semi-infinite rectangle, so we consider LWW equations in such a domain with Dirichlet data on Γ_A denoted $\hat{h}(y,t)$. By using Fourier transform, we look at the problem in frequency domain

$$\frac{\partial^2\hat{\Phi}}{\partial x_1^2}+\frac{\partial^2\hat{\Phi}}{\partial x_2^2}=0 \text{ in } \Omega, \tag{4.1}$$

$$-\omega^2\Phi+g\frac{\partial\hat{\Phi}}{\partial n}=0 \text{ on } \Gamma_S, \quad \frac{\partial\hat{\Phi}}{\partial n}=0 \text{ on } \Gamma_B, \quad \hat{\Phi}=\hat{h} \text{ on } \Gamma_A. \tag{4.2}$$

As in [7], we denote by $\{w_n\}_{n=0}^{+\infty}$ the orthonormal eigenfunctions of the self-adjoint operator $A=-\partial^2/\partial x_2^2$ acting $D(A)$ with

$$D(A)=\{\varphi\in H^2(0,L)\ /\ \frac{\partial\varphi}{\partial x_2}(L)=0 \text{ and } \frac{\partial\varphi}{\partial x_2}(0)=\omega^2\varphi(0)\}. \tag{4.3}$$

The related eigenvalues are denoted λ_n. They are all positive and real except for the first one which is negative. Their corresponding values are uniquely defined (up to a sign) by

$$\lambda_0^2\tanh\lambda_0^2 L=\frac{\omega^2}{L},\quad \lambda_n^2\tan\lambda_n^2 L=\frac{\omega^2}{L}\ n\geq 1. \tag{4.4}$$

$\hat{\Phi}$ is decomposed on the Hilbert basis made of eigenfunctions $\{w_n\}$

$$\hat{\Phi}(\omega,x_1,x_2)=\sum_{n=0}^{+\infty}\hat{\Phi}_n(\omega,x_1)w_n(\omega,x_2). \tag{4.5}$$

By injecting $\hat{\Phi}$ in (4.1), we obtain a family of problems for all n written, on $[0,+\infty[$

$$\frac{\partial^2\hat{\Phi}_n}{\partial {x_1}^2}-\lambda_n\hat{\Phi}_n=0. \tag{4.6}$$

The solution of theses problems are easily obtained using the limit absorption principle to eliminate the ingoing wave and exponential growing waves

$$\hat{\Phi}_0(\omega,x_1)=\big(\hat{h},w_0\big)_{L^2}e^{-i\sqrt{-\lambda_0(\omega)}x_1},\quad \hat{\Phi}_n(\omega,x_1)=\big(\hat{h},w_n\big)_{L^2}e^{-\sqrt{\lambda_n(\omega)}x_1}\ n\geq 1. \tag{4.7}$$

We see that only one mode is propagating, so the approximation made in [7] is to neglect the evanescent waves. The definition of the DtN operator is then straightforward

$$\frac{\partial\hat{\Phi}}{\partial x_1}(\omega,0,x_2)\simeq\frac{\partial\hat{\Phi}_0}{\partial x_1}(\omega,0)w_0(\omega,x_2)=-i\sqrt{-\lambda_0(\omega)}\hat{\Phi}_0(\omega,0)w_0(\omega,x_2). \tag{4.8}$$

Using the same approximation the DtN operator reads

$$-i\sqrt{-\lambda_0(\omega)}\hat{\Phi}_0(\omega,0)w_0(\omega,x_2)\simeq-i\sqrt{-\lambda_0(\omega)}\hat{\Phi}(\omega,0,x_2)\quad\Rightarrow\quad\frac{\partial\hat{\Phi}}{\partial x_1}=-i\sqrt{-\lambda_0}\hat{\Phi}. \tag{4.9}$$

The main question is how to approximate $\lambda_0(\omega)$ to have a stable problem when we get back into time domain. The high order boundary condition (ABC1) presented in [7] reads

$$\sqrt{-\lambda_0(\omega)}\simeq\frac{1}{\sqrt{gL}}+\frac{b\omega^2}{1-a\omega^2}\quad\text{with}\quad a=\frac{11}{60}\frac{L}{g},\quad b=\frac{1}{6}\frac{\sqrt{L}}{\sqrt{g}^3}. \tag{4.10}$$

It has been proven that in the time domain, there is no exponential growth of the solution. This relative weak result can not validate this model for long time simulation. The approximation of $\sqrt{-\lambda_0(\omega)}$ by functions which provides a long time stable and accurate scheme is still an open and difficult question. This motivates the construction of efficient perfectly matched layers.

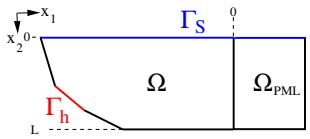

Figure 2: The PML are constructed by adding an artificial layer.

4.2 Construction of Perfectly Matched Layers

In this section, we try to get better absorption by constructing perfectly matched layers (PML), introduced in [2], for this problem. This construction is based on Chew and Weedon's approach for Maxwell's equations [5]. It was already applied to different other equations [3] but never to the LWW system.We first add a rectangular (in 2D) domain Ω_{PML} such that $x_1 \geq L$, on which PML equations are defined, to the physical domain Ω and we set $\widetilde{\Omega}=\Omega\cup\Omega_{PML}$. Then, we define the following change of variable:

$$\tilde{x}_1=\begin{cases} x_1 & \text{if } x_1<0 \\ x_1-\dfrac{\mathrm{i}}{\omega}\displaystyle\int_0^{x_1}\zeta(s)\mathrm{d}s & \text{otherwise} \end{cases} \quad \text{this provides } \frac{\partial}{\partial\tilde{x}_1}=\frac{\mathrm{i}\omega}{\mathrm{i}\omega+\zeta(x_1)}\frac{\partial}{\partial x_1}. \tag{4.11}$$

For sake of simplicity, we suppose in the following that $d=2$, but the computations can be easily extended to the 3D case. In a first step, we replace x_1 by $\tilde{x}_1$ in equations (2.4) and we apply the Fourier transform in time. We get

$$\begin{gathered} \frac{\partial\hat{v}_1}{\partial\tilde{x}_1}+\frac{\partial\hat{v}_2}{\partial x_2}=0 \text{ in } \widetilde{\Omega}, \quad \frac{\partial\widehat{\Phi}}{\partial\tilde{x}_1}=\hat{v}_1 \text{ in } \widetilde{\Omega}, \quad \frac{\partial\widehat{\Phi}}{\partial x_2}=\hat{v}_2 \text{ in } \widetilde{\Omega}, \\ \omega^2\widehat{\Phi}=g\widehat{\vec{v}}\cdot\vec{n} \text{ on } \Gamma_S, \quad \widehat{\vec{v}}\cdot\vec{n}=h \text{ on } \Gamma_h, \quad \widehat{\vec{v}}\cdot\vec{n}=0 \text{ on } \partial\widetilde{\Omega}\setminus\Gamma_S\cup\Gamma_h. \end{gathered} \tag{4.12}$$

By using (4.11), equations (4.12) become

$$\begin{aligned} \mathrm{i}\omega\frac{\partial\hat{v}_1}{\partial x_1}+(\mathrm{i}\omega+\zeta(x_1))\frac{\partial\hat{v}_2}{\partial x_2} &= 0 \text{ in } \widetilde{\Omega}, & \omega^2\widehat{\Phi} &= g\widehat{\vec{v}}\cdot\vec{n} \text{ on } \Gamma_S, \\ \mathrm{i}\omega\frac{\partial\widehat{\Phi}}{\partial x_1} &= (\mathrm{i}\omega+\zeta(x_1))\hat{v}_1 \text{ in } \widetilde{\Omega}, & \widehat{\vec{v}}\cdot\vec{n} &= h \text{ on } \Gamma_h, \\ \mathrm{i}\omega\frac{\partial\widehat{\Phi}}{\partial x_2} &= \mathrm{i}\omega\hat{v}_2 \text{ in } \widetilde{\Omega}, & \widehat{\vec{v}}\cdot\vec{n} &= 0 \text{ on } \partial\widetilde{\Omega}\setminus\Gamma_S\cup\Gamma_h. \end{aligned} \tag{4.13}$$

By applying the inverse Fourier transform in time to (4.13), we get the system in the time domain

$$\begin{aligned} \frac{\partial}{\partial t}\nabla\cdot\vec{v}+\zeta(x_1)\frac{\partial v_2}{\partial x_2} &= 0 \text{ in } \widetilde{\Omega}, & \frac{\partial^2\Phi}{\partial t^2}+g\vec{v}\cdot\vec{n} &= 0 \text{ on } \Gamma_S, \\ \frac{\partial}{\partial t}\vec{v}-\frac{\partial}{\partial t}\nabla\Phi+\zeta(x_1)v_1\vec{e}_1 &= 0 \text{ in } \widetilde{\Omega}, & \vec{v}\cdot\vec{n} &= h \text{ on } \Gamma_h, \\ & & \vec{v}\cdot\vec{n} &= 0 \text{ on } \partial\widetilde{\Omega}\setminus\Gamma_S\cup\Gamma_h. \end{aligned} \tag{4.14}$$

where $\vec{e}_1$ is the unit vector of the x_1-axis. One should remark that no auxiliary unknown are needed to write the continuous problem. This should be compared to what must be done for the wave equation, where, even for a 2D problem auxiliary unknowns must be added. The same remarks can be done for the 3D problem.

4.3 Variational Formulation and Approximate Problem

As for (2.5), from (4.14), after integrating by parts, taking into account the boundary conditions and setting $\widetilde{\Phi}=\partial\Phi/\partial t$ ($\bar{\Phi}=\partial^2\Phi/\partial t^2$ in 3D) [†], we get the following variational problem

$$\frac{\mathrm{d}}{\mathrm{d}t}\int_{\tilde{\Omega}}\vec{v}\cdot\nabla\varphi\mathrm{d}\vec{x}+\int_{\Omega}\zeta(x_1)v_2\vec{e}_2\cdot\nabla\varphi+\frac{1}{g}\frac{\mathrm{d}}{\mathrm{d}t}\int_{\Gamma_S}\zeta(x_1)\widetilde{\Phi}\varphi\mathrm{d}\sigma$$

$$+\frac{1}{g}\frac{\mathrm{d}^2}{\mathrm{d}t^2}\int_{\Gamma_S}\widetilde{\Phi}\varphi\mathrm{d}\sigma=\frac{\mathrm{d}}{\mathrm{d}t}\int_{\Gamma_h}h\varphi\mathrm{d}\sigma,\quad\forall\varphi\in H^1(\Omega),\quad(4.15)$$

$$\frac{\mathrm{d}}{\mathrm{d}t}\int_{\Omega}\vec{v}\cdot\vec{\psi}\mathrm{d}\vec{x}-\int_{\Omega}\nabla\widetilde{\Phi}\cdot\vec{\psi}\mathrm{d}\vec{x}+\int_{\Omega}\zeta(x_1)v_1\vec{e}_1\cdot\vec{\psi}\mathrm{d}\vec{x}=0,\quad\forall\vec{\psi}\in\left[L^2(\Omega)\right]^d.$$

we temporarily introduce an auxiliary variable

$$\vec{w}=\begin{bmatrix}0&0\\0&\zeta(x_1)\end{bmatrix}\vec{v}\Rightarrow\int_{\Omega}\zeta(x_1)v_y\frac{\partial}{\partial y}\varphi\mathrm{d}\vec{x}=\int_{\Omega}\vec{w}\cdot\nabla\varphi\mathrm{d}\vec{x}.\quad(4.16)$$

By applying the mixed formulation defined in section 3.1, we get the following semi-discrete problem in space

$$\frac{\mathrm{d}}{\mathrm{d}t}R_hV+R_hW+\frac{1}{g}\frac{\mathrm{d}}{\mathrm{d}t}D_h^{\gamma,\zeta}\widetilde{U}+\frac{1}{g}\frac{\mathrm{d}^2}{\mathrm{d}t^2}D_h^{\gamma}\widetilde{U}=\frac{\mathrm{d}}{\mathrm{d}t}H,\quad(4.17)$$

$$\frac{\mathrm{d}}{\mathrm{d}t}B_hV=R_h^*\widetilde{U}-B_h^{\zeta,1}V,\quad B_hW=B_h^{\zeta,2}V,\quad(4.18)$$

where V is the discrete vector corresponding to $\vec{v}_h$, $\widetilde{U}$ the discrete vector corresponding to $\widetilde{\Phi}_h$. For $\varphi_i\in U_h^r$ and $\vec{\psi}_i\in\mathbf{V}_h^r$ we define

$$B_{h,ij}^{\zeta,1}=\int_{\Omega}^{LGL}\begin{bmatrix}\zeta(x_1)&0\\0&0\end{bmatrix}\vec{\psi}_j\vec{\psi}_i\mathrm{d}x,\quad B_{h,ij}^{\zeta,2}=\int_{\Omega}^{LGL}\begin{bmatrix}0&0\\0&\zeta(x_1)\end{bmatrix}\vec{\psi}_j\vec{\psi}_i\mathrm{d}x,$$

$$D_{h,ij}^{\gamma,\zeta}=\int_{\Gamma_S}^{LGL}\zeta(x_1)\varphi_j\varphi_i\mathrm{d}x.$$

[†] This change of variable avoids a third-order derivative of Φ in time. The velocity potential can be recovered by a post processing process using $\widetilde{\Phi}$.

We want to keep a fully implicit scheme to achieve unconditional stability . A θ-scheme with $\theta = 1/2$ will be systematically used combined with centered discretizations for the derivatives in time. We get

$$\begin{aligned}\frac{1}{2}R_h(\frac{1}{\Delta t}I_h+B_h^{-1}B_h^{\zeta,2})(V^{n+1}-V^{n-1})+\frac{1}{2g\Delta t}D_h^{\gamma,\zeta}(\widetilde{U}^{n+1}-\widetilde{U}^{n-1})\\ +\frac{1}{g\Delta t^2}D_h^{\gamma}(\widetilde{U}^{n+1}-2\widetilde{U}^{n}+\widetilde{U}^{n-1})=(\frac{\mathrm{d}}{\mathrm{d}t}H)^n,\end{aligned} \tag{4.19}$$

$$(\frac{1}{\Delta t}B_h+B_h^{\zeta,1})V^{n+1}=R_h^*(\widetilde{U}^{n+1}+\widetilde{U}^{n-1})+(\frac{1}{\Delta t}B_h-B_h^{\zeta,1})V^{n-1}. \tag{4.20}$$

As ζ is positive, $\frac{1}{\Delta t}B_h+B_h^{\zeta,1}$ is always invertible. We can replace in (4.19) V^{n+1} by its value defined in (4.20) to have

$$\begin{aligned}(K_h^{\zeta}+\frac{1}{2g\Delta t}D_h^{\gamma,\zeta}+\frac{1}{g\Delta t^2}D_h^{\gamma})\widetilde{U}^{n+1}=(\frac{\mathrm{d}}{\mathrm{d}t}H)^n+\frac{2}{g\Delta t^2}D_h^{\gamma}\widetilde{U}^{n}+R_hB_h^{\zeta}V^{n-1}\\ +(K_h^{\zeta}+\frac{1}{2g\Delta t}D_h^{\gamma,\zeta}-\frac{1}{g\Delta t^2}D_h^{\gamma})\widetilde{U}^{n-1},\end{aligned} \tag{4.21}$$

with

$$K_h^{\zeta}=\frac{1}{2}R_h(\frac{1}{\Delta t}I_h+B_h^{-1}B_h^{\zeta,2})(\frac{1}{\Delta t}B_h+B_h^{\zeta,1})^{-1}R_h^*, \tag{4.22}$$

$$B_h^{\zeta}=(\frac{1}{\Delta t}I_h+B_h^{-1}B_h^{\zeta,2})-(\frac{1}{\Delta t}B_h+B_h^{\zeta,1})^{-1}(\frac{1}{\Delta t}B_h-B_h^{\zeta,1}). \tag{4.23}$$

As $B_h, B_h^{\zeta,1}, B_h^{\zeta,2}$ are $d\times d$ block-diagonal matrices B_h^{ζ} can be easily pre-computed and stored only for the PML domain. One should remark that we intensively use the inverse of the local L^2 mass matrix their particular structures ($d\times d$ block-diagonal) is the key point of the efficiency of the proposed discretization. Experiment have shown that an explicit time discretization of the PML operator (R_hW in (4.17)) leads to unstable schemes. As the original problem ((3.11)-(3.12)) is unconditionally stable, a reasonable time discretization of the PML should keep this property. This motivates the use of a centered implicit scheme for the time discretization of the PML operator. Although we achieved to prove the stability at a continuous level, we were unable to prove a stability result of the fully discretized system of the PMLs.

4.4 Consistency Analysis

The aim of this subsection is to briefly justify the change of variable (4.11). In that purpose, we consider a simplified problem. We take a domain infinite in the positive x_1-direction, Ω being bounded but not Ω_{PML}. We can write the problem using the $\tilde{x}_1$

variable in frequential domain. We consider Dirichlet condition on Γ_h. As seen before, the solution can be written as a superposition of the functions

$$\hat{\Phi}_0(\omega,x_1)=\left(\hat{h},w_0\right)_{L^2}e^{-i\sqrt{-\lambda_0(\omega)}\tilde{x}_1}, \tag{4.24}$$

$$\hat{\Phi}_n(\omega,x_1)=\left(\hat{h},w_n\right)_{L^2}e^{-\sqrt{\lambda_n(\omega)}\tilde{x}_1}\ n\geq 1. \tag{4.25}$$

which gives for every n exponentially decaying waves by writting the solution on x_1

$$\begin{aligned}\hat{\Phi}_0(\omega,x_1)&=\left(\hat{h},w_0\right)_{L^2}e^{-i\sqrt{-\lambda_0(\omega)}x_1}e^{-\sqrt{-\lambda_0(\omega)}\int_0^{x_1}\zeta(s)ds},\\ \hat{\Phi}_n(\omega,x_1)&=\left(\hat{h},w_n\right)_{L^2}e^{-\sqrt{\lambda_n(\omega)}x_1}e^{i\sqrt{\lambda_n(\omega)}\int_0^{x_1}\zeta(s)ds}\ n\geq 1.\end{aligned} \tag{4.26}$$

This shows that we do not have propagating modes in PML and that the solution is preserved in the physical domain. We now need to prove that no exponentially growing modes exists. Indeed the use of the limit absorption principle in (4.6) is not clear anymore, we need to do more to say that no exponential growth occurs.

4.5 Stability Analysis

In order to be efficient,the PML must be well-posed and stable in the sense that it must not produce exponentially growing solutions. This section is devoted to the study of stability by plane wave analysis (as in [8]) in an infinite strip of width L.We suppose that ζ is constant positive and use the frozen coefficient technique proposed by Kreiss and Lorenz [9]. We first redefine the PML by using the classical LWW problem described by (2.1). By using (4.11) and applying the inverse Fourier transform in time, we get

$$\begin{aligned}\frac{\partial^4\Phi}{\partial t^2\partial x_1^2}+\frac{\partial^4\Phi}{\partial t^2\partial x_2^2}+2\zeta\frac{\partial^3\Phi}{\partial t\partial x_2^2}+\zeta^2\frac{\partial^2\Phi}{\partial x_2^2}&=0 \text{ in } \Omega,\\ g\frac{\partial\Phi}{\partial n}+\frac{\partial^2\Phi}{\partial t^2}=0 \text{ on } \Gamma_S,\quad \frac{\partial\Phi}{\partial n}&=0 \text{ on } \Gamma_B.\end{aligned} \tag{4.27}$$

Theorem 1. The solution of (4.27) of the form $\Phi(x_1,x_2,t)=\Phi_{x_2}(x_2)e^{i(\omega t-k_x x_1)}$ are exponentially decaying function in time.

Proof: We set $\Phi(x_1,x_2,t)=\Phi_{x_2}(x_2)e^{i\omega_R t}e^{-\omega_I t}e^{-ik_x x_1}$, where $\omega(k_x)=\omega_R(k_x)+i\omega_I(k_x)$ and $k_x\in\mathbb{R}$. We are looking for solutions such that $\omega_I>0$ in order to obtain exponentially decreasing solutions in time. By plugging the plane wave solution in (4.27), we get the following ODE:

$$-\frac{(i\omega k_x)^2}{(i\omega+\zeta)^2}\Phi_{x_2}(x_2)+\Phi''_{x_2}(x_2)=0, \tag{4.28}$$

with boundary conditions

$$\Phi'_{x_2}(0)=\frac{\omega^2}{g}\Phi_{x_2}(0)\quad\text{and}\quad\Phi'_{x_2}(L)=0. \tag{4.29}$$

Solving (4.28) with (4.29) leads to relation

$$\frac{i\omega k_x}{\zeta+i\omega}\tanh\frac{i\omega k_x L}{\zeta+i\omega}=\frac{\omega^2}{g}. \tag{4.30}$$

For k_x and ζ fixed, $\omega=0$ is one of the solutions of (4.30). For $\omega\neq 0$, (4.30) can be rewritten as

$$(a+ib)\tanh(aL+ibL)=\frac{\omega_R^2-\omega_I^2}{g}+\frac{2\omega_R\omega_I}{g}i, \tag{4.31}$$

where

$$a=\frac{k_x(\omega_I^2+\omega_R^2-\omega_I\zeta)}{(\zeta-\omega_I)^2+\omega_R^2}\in\mathbb{R} \quad \text{and} \quad b=\frac{\omega_R k_x\zeta}{(\zeta-\omega_I)^2+\omega_R^2}\in\mathbb{R}. \tag{4.32}$$

Let us call D_R the set of (a,b) such that ω and k_x verify (4.31). Since $x\tanh x$ is an even function, we restrict ourself to $k_x\geq 0$. Now, we take $\omega_R=0$, which implies that $b=0$. So, if we expand (4.31) and we look at its real part, we have

$$\frac{a(e^{4aL}-1)}{d_1(a,0)}=-\omega_I^2, \tag{4.33}$$

where $d_1(a,b)\ \geq 0\ \ \forall(a,b)\in D_R$. This implies that $a(e^{4aL}-1)\leq 0$ and then $a=0$. Subsequently, $\omega_I=0$. We now suppose that $\omega_R\neq 0$. As above, we expand (4.31) and we look at its real part. We get

$$\frac{e^{4aL}b+4ae^{2aL}\sin(bL)\cos(bL)-b}{d_1(a,b)}=2\omega_R\omega_I. \tag{4.34}$$

After some computations, we get

$$\frac{k_x\zeta g(a,b)}{Ld_1(a,b)}=2\omega_I, \tag{4.35}$$

where

$$g(a,b)=\frac{e^{4aL}}{L}+4ae^{2aL}\frac{\sin(bL)\cos(bL)}{bL}-\frac{1}{L}. \tag{4.36}$$

Since k_x and ζ are positive, we have $\text{sign}(g)=\text{sign}(\omega_I)$. To prove that $g(a,b)$ is always positive, we prove that $\omega_I<0\Rightarrow g(a,b)\geq 0$, so that the assumption $\omega_I<0$ can never be true because of (4.35). For this purpose, we first minor $g(a,b)$. Since

$$\frac{\sin(X)\cos(X)}{X}\geq -1 \quad \forall X\in\mathbb{R}, \tag{4.37}$$

we can write

$$\frac{e^{4aL}}{L}-4ae^{2aL}-\frac{1}{L}\leq g(a,b) \quad \forall(a,b)\in D_R, \tag{4.38}$$

this relation can be rewritten as follows

$$2\frac{e^{2aL}}{L}(\sinh 2aL-2al)\leq g(a,b) \quad \forall(a,b)\in D_R. \tag{4.39}$$

Now, $\omega_I<0\Rightarrow a\geq 0$ implies that $\sinh 2aL-2al>0$ and finally $g(a,b)$ is positive, which contradicts (4.35), and finishes the proof.

5 Numerical Results

In this section we present 2D numerical results obtained with the scheme (4.20)-(4.21). First we validate the PML model by presenting numerical result on a simple rectangle using the same configuration (source and domain) as in [7], second, we present a more realistic situation on a non regular mesh.

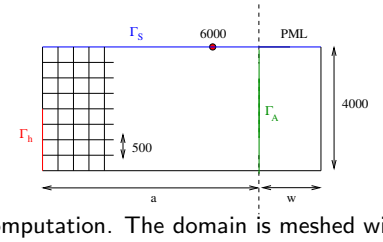

Figure 3: Domain of computation. The domain is meshed with squares of length 500.

The numerical domain of the first numerical experiment is described in figure 3. The length $L=4000$ of the domain will remain constant trough the simulations whereas the width of the PML w and the width of the physical domain a will vary. The mesh will remain fixed, but the order of approximation (r) used on each element of the mesh will vary and so spatial refinements will be done through the increase of order of approximation. We use the parameter $g=10\,m/s^2$ and the source on Γ_h defined by:

$$h(x_1,x_2,t)=A\exp((t-t_0)^2/p^2) \quad \text{with} \quad A=0.169\,m/s, \quad p=11.1408\,s, \quad t_0=35\,s. \tag{5.1}$$

Following [3] we use a damping function in the PML parametrized by σ a positive constant:

$$\zeta(x_1)=\sigma(x_1-a)^2/w^2. \tag{5.2}$$

The choice of a reasonable σ is not discussed here but the quality of the PML depends on the matching of the discretization parameters and the damping function (see figure 4). If σ is too small reflected waves are not damped enough (the reflected waves come from the right boundary of the PML domain). If σ is too big the discretization is not fine enough to correctly take into account the decreasing behavior of the solution which produce reflections as soon as the wave penetrates the PML domain.

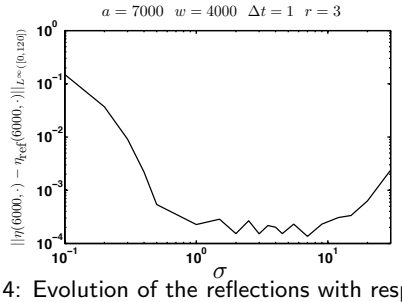

Figure 4: Evolution of the reflections with respect to σ.

At each time step we have to invert the matrix defined by (4.21)-(4.22), to do so we use a standard conjugate gradient. The performance not being a key point to evaluate the efficiency of our PML we do not use preconditioning technique. At each time step the iterative method stops when the norm of the relative residual vector is below 10^{-8}. Figure 5 presents snapshots of the elevation of the surface of the sea without PML on a large domain and with PML. We clearly see the decaying behavior of the water waves when it enters the PML.

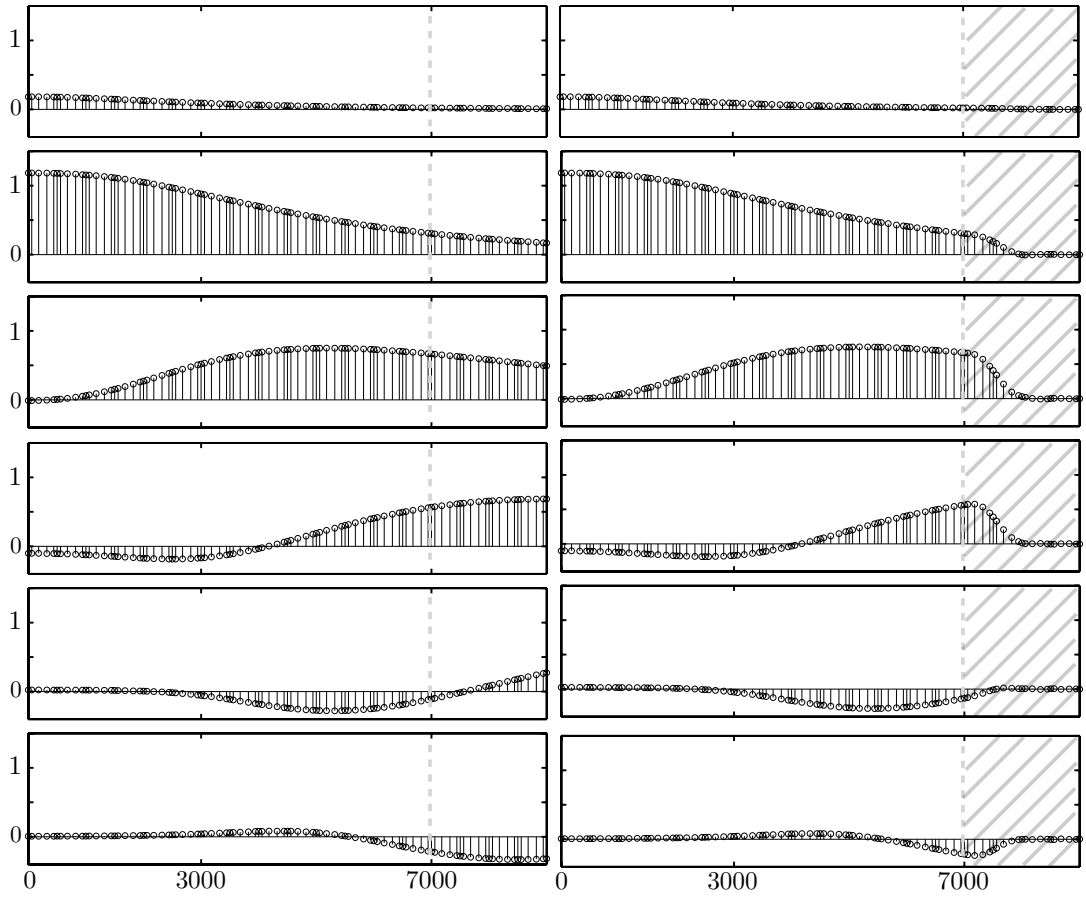

Figure 5: Snapshots at $t=25s,50s,75s,100s,125s$ and $150s$ of the elevation for two different cases. Left: on a sufficiently large domain. Right: with PML, the dashed line separates the physical domain from the PML domain.

To study more precisely the efficiency of the PML model we compute the difference of elevation $\eta(x_1,t)$ at $x_1=6000$, obtained with different sizes of PML ($w=4000$ or $w=8000$) and different orders ($r=1$ to $r=5$) of discretization between an elevation computed on a larger domain ($a=64000$) with the ABC1. To filter the discretization error from the

reflection error, the elevation computed on the larger domain is always obtained with the same time step and order of elements as the simulation (with PML) it is compared with. A simple homogeneous Neumann condition is used on the right boundary when PML are used. When $w=0$, i.e. when no PML are used, we use the ABC1 on Γ_A. As the ABC1 explodes in long time simulation (see figure (6)) we compute the infinite norm of the reflection for short time simulation (between $t=0$ and $t=120$) and compare PML and ABC1, the result are shown figure 7.

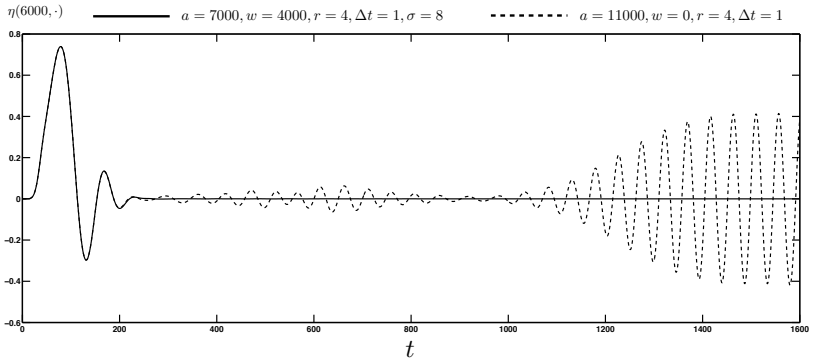

Figure 6: Elevation at $x_1=6000$ using PML and ABC1. The ABC1 shows a linear growing behavior in time.

On the left graph of figure 7 we observe a numerical locking when we increase the order of approximation. The time step is not small enough to correctly take into account the decreasing behavior of the wave. Order 1 and 2 elements are also not able to correctly take into account this behavior. On the right graph a smaller time step is used. The numerical locking is shifted and the reflections decreased with the order of approximation. In both cases, the reflections decrease with the increase of the layer's width (w=4000 to w=8000), note also that the reflections generate by the ABC1 are independent of the discretization parameters. These reflections are more important than those produce by the PML as soon as the discretization parameters are well chosen.

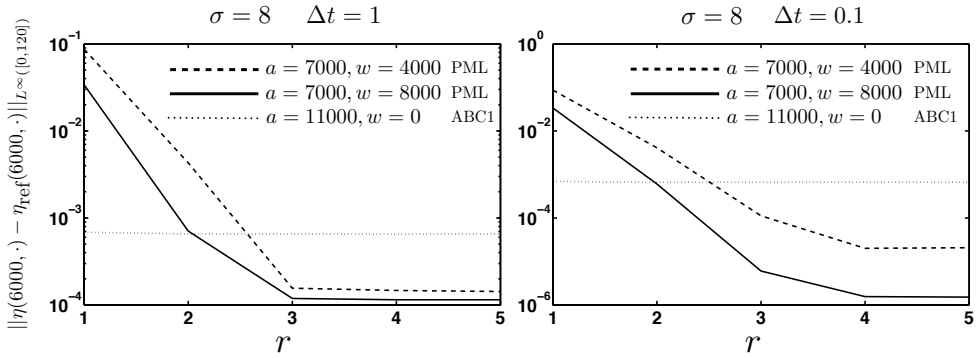

Figure 7: Reflections with respect to the order r for different time steps Δt for a fixed $\sigma=8$.

Previous results and practical experiment show that whereas the ABC1 are cheap in term of computation time compared to the PML they do not provide satisfactory result in term of stability. PML also offer a better precision if one adjusts the discretization parameters.

To conclude the numerical result section we present a more realistic simulation. We consider a sea bottom with an obstacle (see figure 8). PML are used to bound the domain on the left and on the right. The mesh is composed of triangles that are cut into quadrangles in order to apply the mixed finite element technique. The left side of the domain represents the beginning of a coast, that is the region where the linearized water waves equation may be no longer valid. On figure 9 we present different snapshots of the simulation on which the elevation η and the derivative in time of the velocity potential ($\tilde{\Phi}$) are represented.

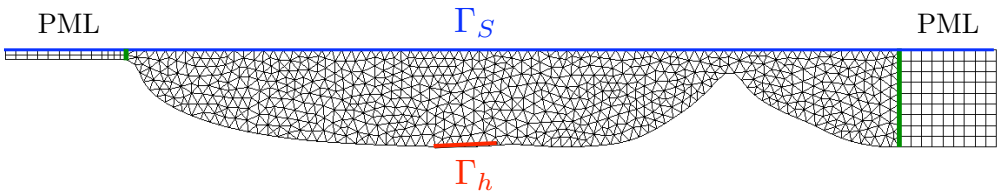

Figure 8: Mesh of the computational domain surrounded by PML. The triangles are cut into quadrangles to apply the mixed spectral elements method.

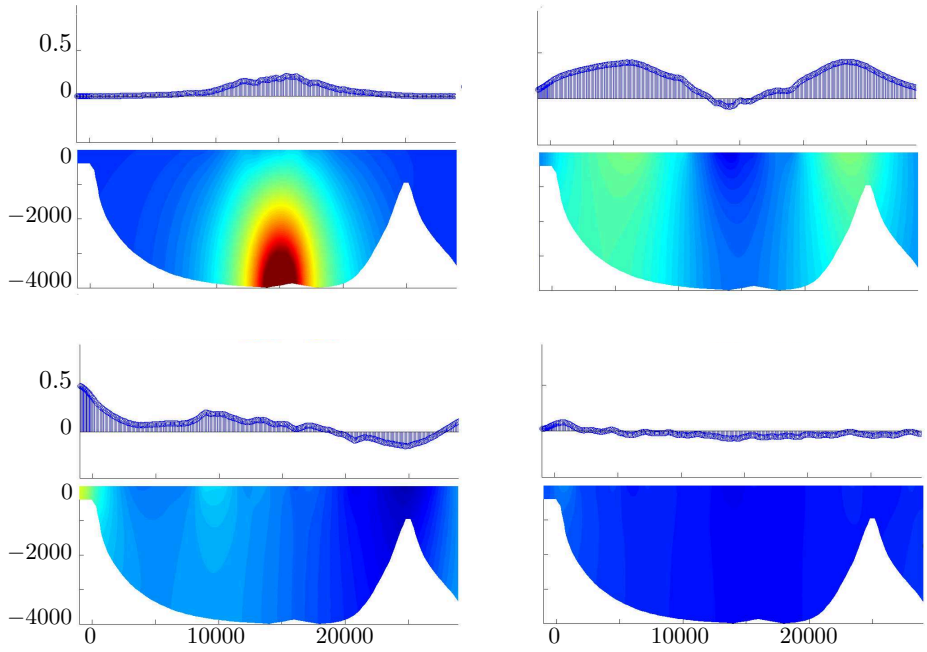

Figure 9: Snapshot at t=30, t = 90, t=150 and t = 340 of the elevation (upper part) and the time derivative of the velocity potential (lower part). The domain is surrounded by PML.

6 Conclusion

We constructed an algorithm of resolution for the linearized water waves problem in 2D by using a mixed spectral element method. This construction can be extended to the 3D case provided a possibility of meshing the domain by hexahedra. The statement of instability of absorbing boundary conditions for unbounded domains motivated the construction of an original perfectly matched layer. We analyzed the stable character of our perfectly matched layer in the case of constant coefficient by using Fourier technique. Numerical results showed the stability of our approach for long time simulation and its capability to model unbounded complex domains.

References

[1] J. L. Hammack, *A note on tsunamis: their generation and propagation in an ocean of uniform depth* J . Fluid Mech. (1973), wol. 60, part 4, pp. 769-799

[2] J.-P. Bérenger, *A perfectly matched layer for the absorption of electromagnetic waves*, J. Comput. Phys. **114** (2), pp. 185–200, 1994.

[3] G. Cohen, *Higher Order Numerical Methods for Transient Wave Equations*, Springer, 2001.

[4] G. Cohen, S. Fauqueux *Mixed spectral finite elements for the linear elasticity system in unbounded domains.* SIAM J. Sci. Comput. **26**, no. 3,pp. 864-884,2005.

[5] W. C. Chew, W. H. Weedon, *A 3D perfectly matched medium from modified Maxwell equations with stretched coordinates*, IEEE Microwave and Optic. Tech. Letters, **7** (13), pp. 599-604, 1999.

[6] M. Duruflé *Intégration numérique et éléments finis d'ordre élevé appliqués aux équations de Maxwell en régime harmonique*, PhD Thesis, Université de Paris IX Dauphine (2006).

[7] K. Dgaygui, P. Joly, *Absorbing boundary conditions for linear gravity waves*, SIAM J. Appl. Math., **54**, no. 1, pp. 93–131, 1994.

[8] E. Becache, S. Fauqueux, P. Joly, *Stability of perfeclt matched layers, group velocities and anistropic waves*J. Comput. Phys.**188** (2), pp. 399-433, 2003.

[9] H-O. Kreiss, J. Lorenz *Initial-boundary value problems and the Navier-Stokes equations.* Pure and Appl. Math. **136** 1989